AIAA 01–0717

# Static Aero-elastic Computation with a Coupled CFD and CSD Method

J. Cai, F. Liu
*Department of Mechanical and Aerospace Engineering*
*University of California, Irvine, CA 92697-3975*

H.M. Tsai, A.S.F. Wong
*DSO National Laboratories*
*20 Science Park Drive, Singapore 118230*

**39th AIAA Aerospace Sciences Meeting and Exhibit**
**January 8–11, 2001/Reno, NV**

# Static Aero-elastic Computation with a Coupled CFD and CSD Method

J. Cai*, F. Liu†
*Department of Mechanical and Aerospace Engineering*
*University of California, Irvine, CA 92697-3975*

H.M. Tsai‡, A.S.F. Wong §
*DSO National Laboratories*
*20 Science Park Drive, Singapore 118230*

**The objective of this paper is to assess the computational effectiveness of an integrated scheme for static aero-elastic problems that makes use of methods of Computational Fluid Dynamics (CFD) and Computational Structural Dynamics (CSD). The CFD algorithm is based on an unsteady, parallel, multi-block, multi-grid finite-volume, Euler/Navier-Stokes solver previously used for time accurate unsteady flow computations. This is coupled with a structures solver and a deforming mesh algorithm in time using a fully implicit dual-time stepping method. Grid deformation cost is small by using algebraic techniques. The computational effort needed for updating the aerodynamic shape due to elastic deformation is rendered negligible by using modal approximations pre-determined by using a finite element method or experimentally. Since time accuracy is irrelevant, static elastic equations are used rather than the dynamic structural equations. The structural and flow equations interact at every iteration in time. For illustrative purposes a generic wing was studied using both Euler and Navier-Stokes computations. Results show that computational cost of this method is comparable to a CFD study of a rigid structure. Comparisons are made of computed pressure distributions for the rigid and flexible wings at the same flight conditions. Comparisons are also made between the results of Euler and Navier-Stokes computations.**

## I. Introduction

CFD analysis of wings and aircraft are usually performed with rigid body assumption for the wing and aircraft structures. In this paper, we modify a time accurate coupled CFD-CSD method developed for flutter simulations to perform static aeroelastic calculations.

The authors developed an integrated CFD-CSD simulation code[1] for flutter calculations based on a parallel, multiblock, multigrid flow solver for the Euler/Navier-Stokes equations. Structural modal dynamic equations were solved simultaneously in a strongly coupled fashion with the Navier-Stokes equations by a fully implicit time marching method. A dual-time stepping algorithm was used to achieve time accuracy and allow simultaneous integration of the flow and structural equations without any time delay. A novel moving mesh method was developed to dynamically move/deform the computational grid at each time step and a spline matrix method was used to provide the interpolation between the CFD and CSD grids.

In principle, the above method could be directly used to perform static aeroelastic calculations if the computation is allowed to continue for a long time until it reaches a steady state, given appropriate initial and boundary conditions. However, this leads to unacceptably long computational time because the coupled system may oscillate many cycles before settling down at an equilibrium position. Since time accuracy is of no interest for static aeroelasticity, the original time-accurate method can be modified so that convergence to the final equilibrium state can be accelerated using non-time-accurate algorithms including modifications of the structural dynamic equations as long as they do not affect the converged equilibrium solution. In order to access the effectiveness of such an approach by an integrated CFD-CSD method, the AGARD 445.6[2,3] wing previously studied for its flutter characteristics is here used as a test case for static aeroelastic calculations. It is found that neglection of the inertial terms in the structural equations, in other words, use of only the static elastic equations, give the best convergence provided a relaxation procedure is used to guarantee robustness of the method. Convergence histories of the different methods and comparisons of the computed results by the Euler and the Navier-Stokes equations for the elastic wing will be shown along with solutions for the rigid wing.



*Visiting Research Specialist, Associate Professor, Northwestern Polytechnical University, Xi'an, China.

†Associate Professor. Senior Member AIAA.

‡Senior Member of the Technical Staff. Member AIAA. Currently Adjunct Associate Professor, National University of Singapore, Singapore 119260.

§Member of Technical Staff.

## II. The Unsteady Navier-Stokes Solver with a Moving Mesh Algorithm

The authors[1] developed an integrated Aero-Structural dynamics code later called ACES3D[4] for flutter simulations of wings and aircraft. This code is based on a parallel multiblock, multigrid unsteady Euler/Navier-Stokes solver. Time-accuracy is achieved by using the dual-time method. After being discretized in space by a finite volume method, the time dependent Navier-Stokes equations can be written in the following semi-discrete form

$$\frac{dw}{dt} + R(w) = 0 \tag{1}$$

where $w$ is the vector of flow variables at each mesh point, and $R$ is the vector of the residuals, consisting of the spatially discretized flux balance of the Navier-Stokes equations. A second order accurate fully implicit scheme is then used to integrate the above equation in time,

$$\frac{3w^{n+1} - 4w^n + w^{n-1}}{2\Delta t} + R(w^{n+1}) = 0 \tag{2}$$

This implicit scheme is A-stable. We can reformulate (2) into the following

$$\frac{dw}{dt^*} + R^*(w) = 0 \tag{3}$$

where

$$R^*(w) = \frac{3}{2\Delta t}w + R(w) - \frac{2}{\Delta t}w^n + \frac{2}{2\Delta t}w^{n-1} \tag{4}$$

$t^*$ is a pseudo-time. The solution of the implicit equation (2) is now made equivalent to the steady state solution of (3) with the pseudo time $t^*$. We can then apply all the acceleration techniques including the multigrid method that are already implemented in the steady NSAERO to solving Equation (3). Once the solution to Equation (3) converges in pseudo time, we achieve the time accurate solution to Equation (2) for one time step.

Time accurate calculations for three-dimensional problems are still very time consuming with even the best algorithms available at the current time. In order to keep the computational time within realistic limits for large unsteady calculations, the code is also parallelized by using domain decomposition and MPI to take advantage of parallel computers or networked clusters of workstations. The flow field is partitioned into multiple blocks which are distributed over a number of processors available on a parallel computer or networked workstations. As shown in reference[1] a speedup factor of 25 was achieved with 32 processors in a PC clusters using regular 100Mb/s network.

A novel moving grid algorithm, AIM3D, which remeshes the moving configuration adaptively in each block of grids, is also implemented in a parallel fashion and combined with the flow solver to handle flow problems with arbitrary motion of domain boundaries. The moving grid algorithm within each block is based on the method of arc-length based transfinite interpolation which is performed independently on local processors where the blocks reside. A spring network approach is used to determine the motion of the corner points of the blocks which may be connected in an unstructured fashion in a general multi-block method. A smoothing operator is applied to the points of the block face boundaries and edges in order to maintain grid smoothness and grid angles. The details of this moving grid method is described in[5]

## III. The CSD Model and Its Solution

Modal equations are used to calculate the structural deformation under an aerodynamic forcing. For each mode $i$, the modal dynamic equation is written in the following form

$$\ddot{q}_i + 2\zeta_i\omega_i\dot{q}_i + \omega_i^2 q_i = Q_i \tag{5}$$

where $q_i$ is the generalized normal mode displacement, $\zeta_i$ is the modal damping, $\omega_i$ is the modal frequency, and $Q_i$ is the generalized aerodynamic force. The structural displacement vector can be written as a summation of $N$ modal shapes extracted from a full finite element analysis of the structure.

$$u_s = \sum_{i=1}^{N} q_i h_i \tag{6}$$

where $h_i$ are the modal shapes.

Equation (5) is converted into a first order system of equations for each $i$ and integrated in time by a second-order fully implicit scheme in time.

$$\frac{3z_{1i}^{n+1} - 4z_{1i}^n + z_{1i}^{n-1}}{2\Delta t} = -R_{1i}(z_{1i}^{n+1}, z_{2i}^{n+1}, Q_i^{n+1}) = \omega_i(-\zeta_i + \sqrt{\zeta_i^2 - 1})z_{1i}^{n+1} + \frac{(-\zeta_i + \sqrt{\zeta_i^2 - 1})}{2\sqrt{\zeta_i^2 - 1}}Q_i^{n+1} \tag{7}$$

$$\frac{3z_{2i}^{n+1} - 4z_{2i}^n + z_{2i}^{n-1}}{2\Delta t} = -R_{2i}(z_{1i}^{n+1}, z_{2i}^{n+1}, Q_i^{n+1}) = \omega_i(-\zeta_i - \sqrt{\zeta_i^2 - 1})z_{2i}^{n+1} + \frac{(\zeta_i + \sqrt{\zeta_i^2 - 1})}{2\sqrt{\zeta_i^2 - 1}}Q_i^{n+1} \tag{8}$$

where $z_{1i}$, $z_{2i}$ are the complex representation of the modal displacement and velocity for the $i$-th mode.

The variables $z_{1i}$, $z_{2i}$, and $Q_i$ in the above equations are coupled through the flow equations. The deformation of the wing, i.e., $z_{1i}$, $z_{2i}$ influences the flow field, and thus the aerodynamic force $Q_i$. Conversely, the aerodynamic force $Q_i$ determines the deformation of the wing. Therefore, the above equations for the time marching of the structural equations must be solved simultaneously with Equation (2) for the Navier-Stokes equations.

It is very convenient to reformulate Equations (7) and (8) into an identical pseudo time format as Equations (3) and (4), i.e.,

$$\frac{dz_{1i}}{dt^*} + R^*_{1i}(z_{1i}, Q_i) = 0 \tag{9}$$

$$\frac{dz_{2i}}{dt^*} + R^*_{2i}(z_{2i}, Q_i) = 0 \tag{10}$$

where

$$\begin{aligned} R^*_{1i}(z_{1i}, Q_i) &= \frac{3}{2\Delta t} z_{1i} + R_{1i}(z^{n+1}_{1i}, z^{n+1}_{2i}, Q^{n+1}_i) \\ &\quad -\frac{2}{\Delta t} z^n_{1i} + \frac{1}{2\Delta t} z^{n-1}_{1i} \end{aligned} \tag{11}$$

$$\begin{aligned} R^*_{2i}(z_{1i}, Q_i) &= \frac{3}{2\Delta t} z_{2i} + R_{2i}(z^{n+1}_{1i}, z^{n+1}_{2i}, Q^{n+1}_i) \\ &\quad -\frac{2}{\Delta t} z^n_{2i} + \frac{1}{2\Delta t} z^{n-1}_{2i} \end{aligned} \tag{12}$$

Equations (3), (11) and (12) can be regarded as one single system of time dependent equations in the pseudo time $t^*$ which can be solved by existing efficient explicit time marching methods until a steady state is reached. Once the computation reaches a steady state in the pseudo time $t^*$, the solutions to Equations (3), (11) and (12) then become the time accurate solution of the implicit fully coupled CFD-CSD Equations (2), (7) and (8) in one physical time step without any time lag between the CFD and CSD equations.

# IV. Interfacing between the CSD and CFD Grids

Most CFD codes use different algorithms and different computational grids for the flow and the structures as is the case in the present work. Consequently, interpolation of computational grids and aerodynamic loads must be performed between the two systems. A spline matrix method is used in the present work to relate the structural grid to the aerodynamic grid. The displacement vector defined on the structural grid $\{u_s\}$ can be related to the displacement vector on the aerodynamic grid $\{u_a\}$ via a spline matrix $[G]$,

$$\{u_a\} = [G]\{u_s\} \tag{13}$$

Once the structure equations are solved, the displacements on the structural grid $\{u_s\}$ is transformed to the displacement on the aerodynamic grid $\{u_a\}$ by the above equation, from which the deforming grid code AIM3D discussed in Section 3 can then be used to regenerate the volume grid in the flow field for CFD computations. Once the flow equations are solved, the aerodynamic loading on the CFD grid $\{F_a\}$ can then be transformed to the aerodynamic loading on the structural grid $\{F_s\}$ via the following equation based on the principle of virtual work.

$$\{F_s\} = [G]^T\{u_a\} \tag{14}$$

where $[G]^T$ is the transpose of $[G]$. Equation (14) guarantees the conservation of energy between the flow and the structural systems due to the fact that it is derived by the principle of virtual work. The $[G]$ matrix is pregenerated and stored in the code.

# V. Modifications for Static Elastic Calculations

In the integrated aero-structure flutter simulation system described in,[1] equations (3), (11) and (12) are integrated together to obtain time accurate solutions to the coupled aero-structure system. In principle, it can be directly used to calculate static aeroelasticity. Given a proper flight condition with its associated boundary conditions, we may start with an arbitrary initial condition and resolve the dynamic motion of the wing under the influence of the aerodynamics due to the wing itself. Provided the system is intrinsically stable, it is expected that the computations will reach a steady state after a sufficiently long time. This final steady state will then be the needed equilibrium point of the static aeroelastic system.

However, if the above direct simulation is used, the time needed to reach a steady state is unacceptably long since the system needs, in general, many cycles to reach a steady state. In order to reduce this long time needed to reach steady state, one can artificially increase the structural damping coefficients $\zeta_i$. Computations show, however, that this approach is still less than satisfactory. Since only the final equilibrium solution is needed, an alternative is to sacrifice the time accuracy in exchange for speed to steady state. For this purpose, the original time accurate code has been modified to include an option for static aero-elastic calculations, in which the time accurate equations (3), (11) and (12) are integrated together without the source terms. Information between the structural and aerodynamic equations are exchanged within each pseudo time step until the computation reaches a steady state. In addition, the inertial terms in the modal structural equations $\ddot{q}$ is removed from the equation to prevent cyclic oscillation of the wing. This is equivalent to updating the wing shape at the end of each time step for the Navier-Stokes equations by using only the static elastic equations for the structures.

The above method works well for situations with small deformation of the wing. In cases where large deformation may occur, computations may not converge. In order to prevent such situations, a relaxation procedure is introduced in which the newly calculated structural displacement at each time step is weighted against the old displacement in the previous time step before it is passed to the Navier-Stokes solver, ie.

$$q^{n+1} = \alpha \overline{q^{n+1}} + (1-\alpha) q^n \tag{15}$$

where $0 < \alpha < 1$ is a relaxation parameter. This

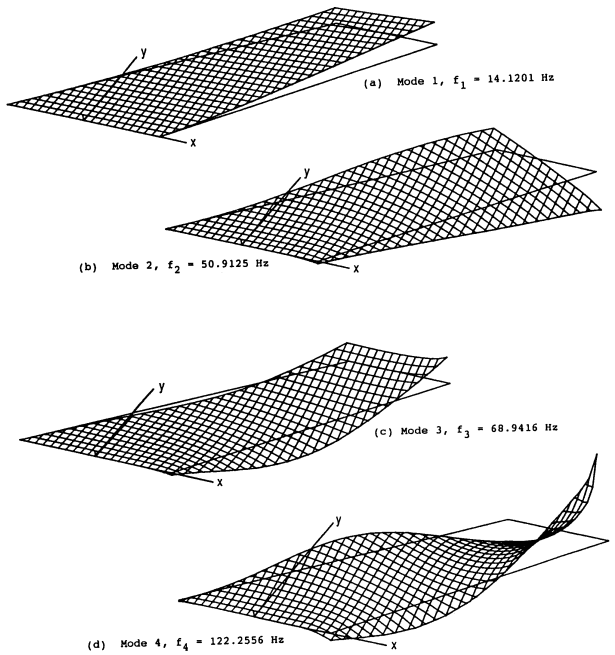


**Fig. 1 Modal deflections for the 445.6 Wing**

relaxation procedure has little negative effect on the convergence rate but avoids situations of diverging computations.

## VI. Computational Results

The AGARD 445.6 wing[2,3] was studied for its flutter characteristics.[1] In the present work, however, it is used as a test case for static aeroelasticity. This wing is a semispan model made of the NACA 65A004 airfoil that has a quarter-chord sweep angle of 45 degrees, a panel aspect ratio of 1.65, and a taper ratio of 0.66. We consider the weakened wing model as listed in Reference.[2] The wing is modeled structurally by the first four natural vibrational modes shown in Figure 1 as taken from Reference.[3] Those are identified as the first bending, first torsion, second bending, and second torsion modes, respectively, by a finite-element analysis. Figure 2 shows the perspective view of the 32-block O-grid used in the computation. Thick lines show the block boundaries.

We first use the time-accurate coupled CFD-CSD method starting from uniform flow of $M_\infty = 0.85$ with the wing set at an angle of attack of 5°. Figure 3 shows the time history of the computed lift and moment coefficients with 0%, 50%, and 80% structural damping ($\zeta_i$=0, 0.5, and 0.8, respectively.) the computation with the zero damping shows a pronounced oscillatory behavior of the wing that indicates the need of long computations before the wing will settle down to its equilibrium state. Adding a large amount of damping significantly suppresses this oscillatory behavior, but still need more than several tens of time accurate steps in order to reach a steady state.

Figure 4 shows the history of lift and moment coef-

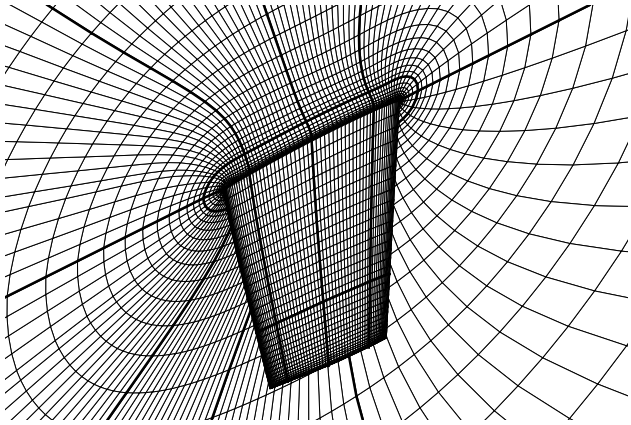

**Fig. 2 Perspective view of the O-grid. The thick lines show the block boundaries. The off-body grid is at the plane of symmetry.**

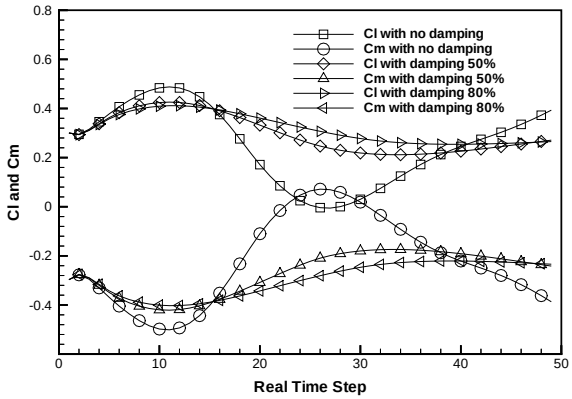


**Fig. 3 History of $C_l$ and $C_m$ in time for different amounts of structural damping, Euler computation**

ficients with the relaxation method for both the rigid wing and the elastic wing. Notice that the x-axis is now the iteration steps, that is the total number of pseudo time steps, rather than time accurate real time steps in Figure 3. In this method, the inertial and damping terms in the structural equations are completely neglected, therefore, the structural equations are solved with the flow equations without time accuracy. A value of 0.5 is used for the relaxation parameter given in Equation (15). It can be seen that the solutions converge within about 100 time steps. No extra work is needed for the elastic wing calculation vs. a steady state calculation of the rigid wing although the final converged lift and moment coefficients are different due to the deformation of the wing compared to the rigid wing.

Figure 5 shows the same convergence histories for the Navier-Stokes calculations. Again, there is no significant convergence differences between the computation of the elastic wing and that of the rigid wing. Figure 6 shows the history of residuals of the calculations of the rigid wing and the elastic wing with no relaxation and a relaxation parameter $\alpha = 0.5$. It

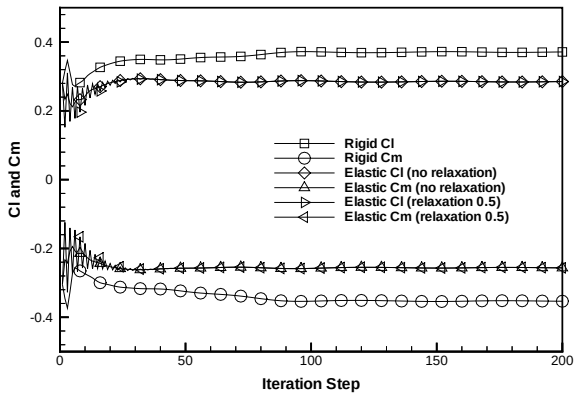


**Fig. 4 History of $C_l$ and $C_m$ for different values of the relaxation parameter $\alpha$, Euler computation**

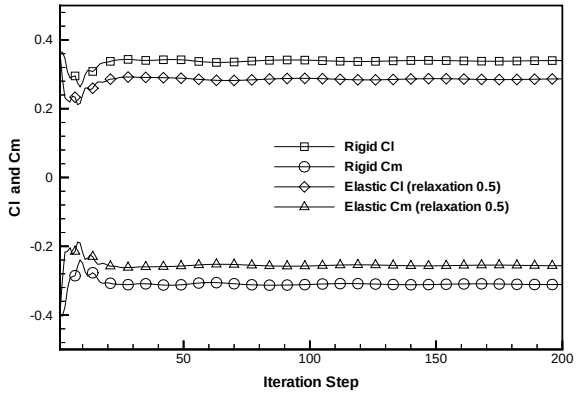


**Fig. 5 History of $C_l$ and $C_m$ for different values of the relaxation parameter $\alpha$, Navier-Stokes computation**

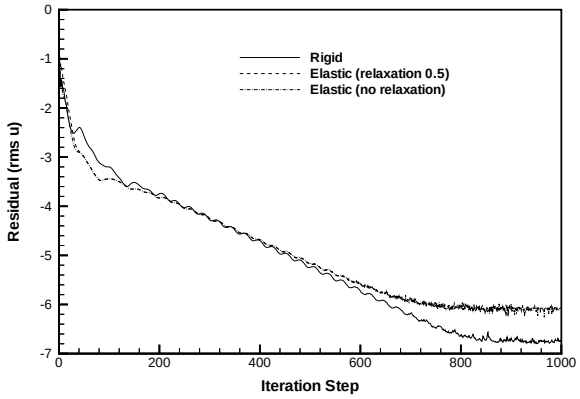


**Fig. 6 Comparison of convergence histories for rigid and elastic wings, Euler computation**

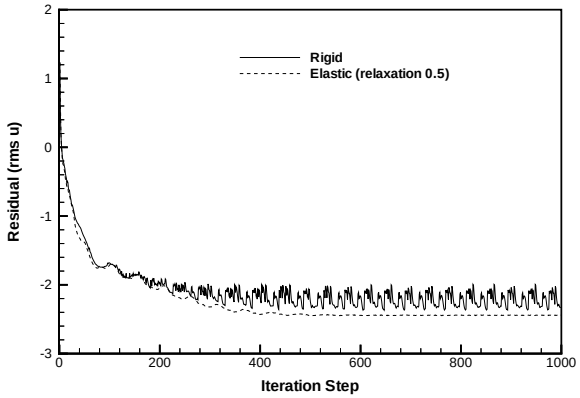


**Fig. 7 Comparison of convergence histories for rigid and elastic wings, Navier-Stokes computation**

can be seen that for this case the calculations for the elastic wing converges actually faster then that for the rigid wing. This is because the existence of a small separation bubble near the tip of the wing at the 5° of angle of attack for the rigid wing. For the flexible wing, the elastic deformation under the aerodynamic loading gives an outwash, reducing the effective angle of attack near the wing tip. This makes the flow less severe near the wing tip and thus gives a better convergence level.

It is also seen from figures 4 and 6 that there is no difference between the solutions with and without relaxation as long as the solutions converge. Under larger angles of attack, however, computations without the relaxation do not converge due to initial large deformations of the wing. Figure 7 shows the convergence history for the Navier-Stokes computations. They are qualitatively the same as those for the Euler computations.

Figures 8 and 9 show the comparison of the pressure distributions at 34% and 67%, respectively, calculated by the Euler and the Navier-Stokes equations for the rigid wing. Significant differences exist at the 67% location, where as mentioned ealier, the Euler calculations tend to predict an inviscid separation bubble. This is confirmed by the pressure contours shown in Figures 10, 11, 12, and 13.

Figures 14 and 15 show the comparison of the pressure distributions at 34% and 67%, respectively, calculated by the Euler and the Navier-Stokes equations for the elastic wing. This time, the differences between the Euler and the Navier-Stokes equations are smaller except that the Euler equations tend to predict larger suction peaks compared to the Navier-Stokes equations. The pressure contous on the wing shown in Figures 16, 17, 18, and 19 confirm the same observations.

Figure 20 plots the vertical deflection of the wing at the leading and trailing edges due to aerodynamic loading along the wing span relative to the root location. It can be seen that the trailing edge has a larger upward deflection than the leading edge, indicating a washout of the wing under the aerodynamic loading. The Euler solution predicts a larger washout than the

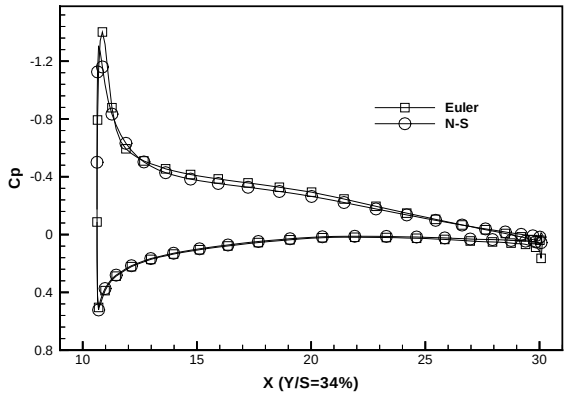


**Fig. 8 Comparison of $C_p$ distributions at 34% span by Euler and Navier-Stokes equations for the rigid wing**

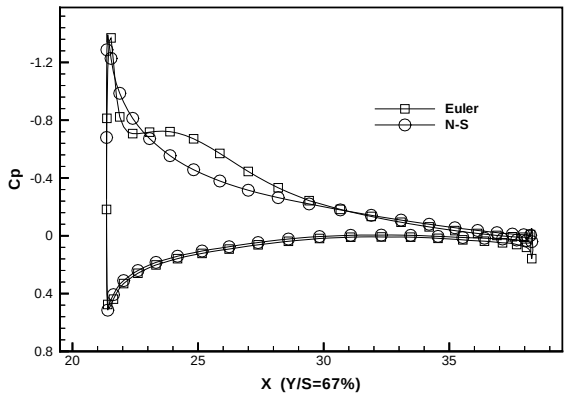


**Fig. 9 Comparison of $C_p$ distributions at 67% span by Euler and Navier-Stokes equations for the rigid wing**

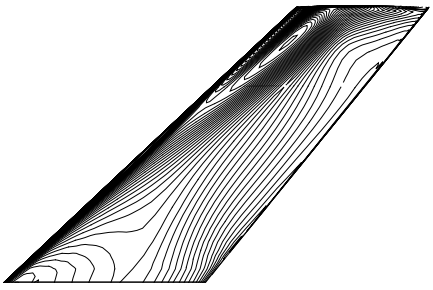

**Fig. 10 Pressure contours on upper surface of rigid wing, Euler solution**

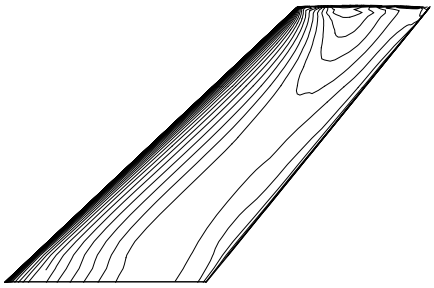

**Fig. 11 Pressure contours on lower surface of rigid wing, Euler solution**

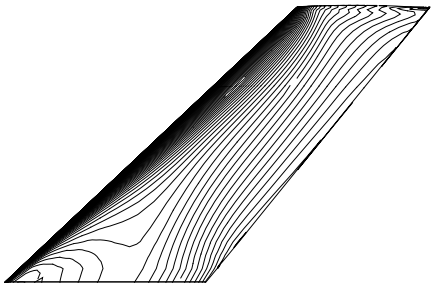

**Fig. 12 Pressure contours on upper surface of rigid wing, Navier-Stokes solution**

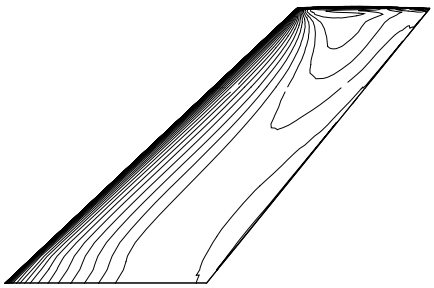

**Fig. 13 Pressure contours on lower surface of rigid wing, Navier-Stokes solution**

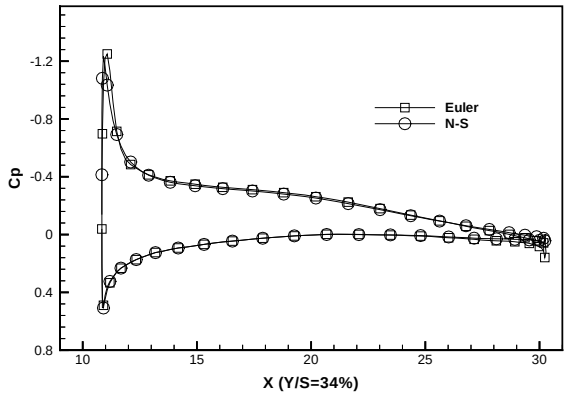


**Fig. 14 Comparison of $C_p$ distributions at 34% span by Euler and Navier-Stokes equations for the elastic wing**

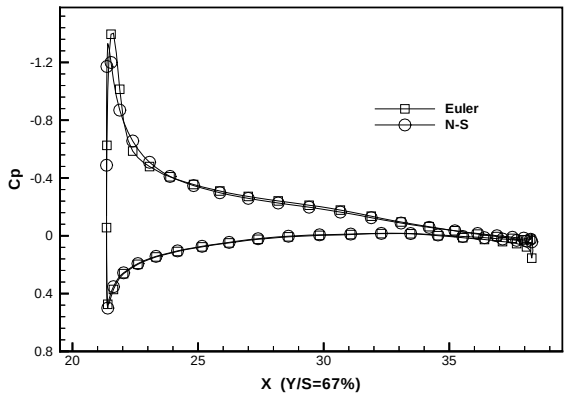


**Fig. 15 Comparison of $C_p$ distributions at 67% span by Euler and Navier-Stokes equations for the elastic wing**

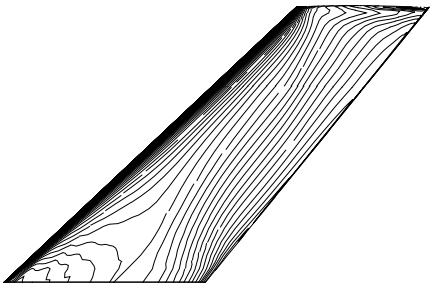

**Fig. 16 Pressure contours on upper surface of elastic wing, Euler solution**

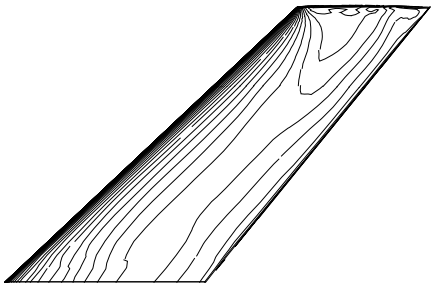

**Fig. 17 Pressure contours on lower surface of elastic wing, Euler solution**

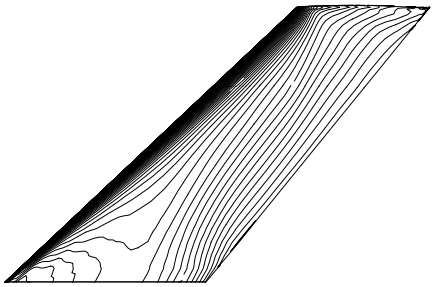

**Fig. 18 Pressure contours on upper surface of elastic wing, Navier-Stokes solution**

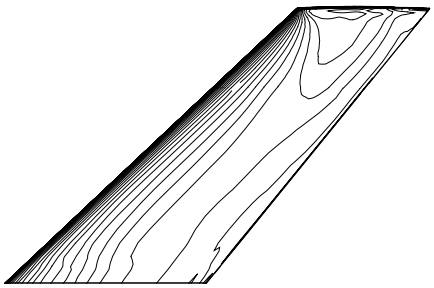

**Fig. 19 Pressure contours on lower surface of elastic wing, Navier-Stokes solution**

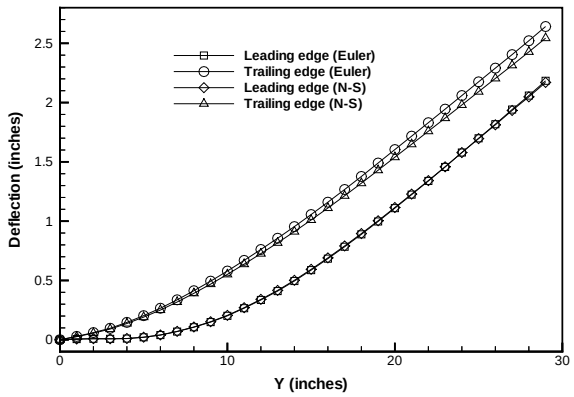


**Fig. 20 Vertical deflection of wing along span relative to the wing root**

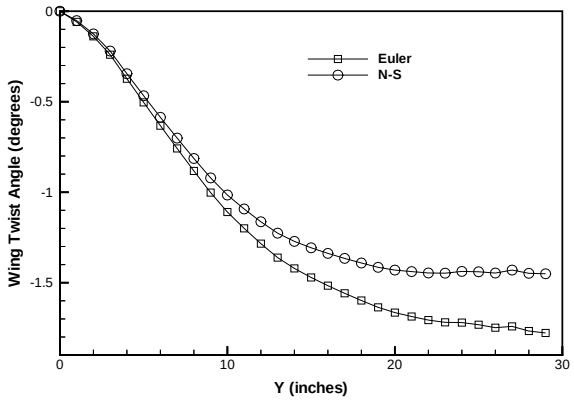


**Fig. 21 Twist of wing along span relative to the wing root**

Naver-Stokes equations. This is clearly seen in Figure 21 where the twist angles of the wing along the span is plotted. The Euler calculations show a larger downward twist than the Navier-Stokes solutions.

## VII. Concluding Remarks

A parallel integrated CFD-CSD simulation program has been developed for analysis of static aeroelasticity. This program consists of a three-dimensional, parallel, multi-block, multigrid, unsteady Navier-Stokes solver, a parallel dynamic grid deformation code, a CSD solver strongly coupled with the flow solver using dual time stepping, and a spline matrix method for interfacing the CFD and CSD grid and aerodynamic loading variables.

Convergence to equilibrium state of a static aeroelastic system is accelerated by using a strongly coupled relaxation technique that is both robust and fast. The 445.6 wing is used as a test case. It is found that the time for obtaining a static aeroelastic solution is practically the same as obtaining the solution for a rigid body. Both Euler and Navier-Stokes solutions have been obtained. Significant differences exist between solutions of rigid wing and the flexible wing, and also between solutions with the Euler and the Navier-Stokes equations. A static aeroelastic computation must be performed in place of rigid wing calculations in order to get accurate predictions of the aerodynamic performance of the wing.

## VIII. Acknowledgement

Computations of this work has been performed on the AENEAS parallel computer system and the SGI parallel computer system in UC Irvine.

## References

[1]Liu, F., Cai, J., Zhu, Y., Wong, A. S. F., and Tsai, H.-M., "Calculation of Wing Flutter by a Coupled CFD-CSD Method," AIAA Paper 00–0907, Jan. 2000.

[2]Yates Jr., E. C., Land, N. S., and Foughner, J. T., "Measured and Calculated Subsonic and Transonic Flutter Characteristics of a 45° Swepteback Wing Planform in Air and in Freon-12 in the Langley Transonic Dynamics Tunnel," NASA TN D-1616, March 1963.

[3]Yates Jr., E. C., "AGARD Standard Aeroelastic Configurations for Dynamic Response, I – Wing 445.6," AGARD Report 765, Aug. 1987, also NASA TM 100492.

[4]Wong, A. S. F., Tsai, H.-M., and Liu, F., "ACES3D: A Computer Program for Aerodynamic Computation of Elastic Structures in 3-Dimensions," Dso technical report and manual, DSO National Laboratories, 20 Science Park Drive, Singapore 118230, March 2000.

[5]Wong, A. S. F., Tsai, H.-M., Cai, J., Zhu, Y., and Liu, F., "Unsteady Flow Calculations with a Multi-Block Moving Mesh Algorithm," AIAA Paper 00–1002, Jan. 2000.